STAR Protocols

CellPress
OPEN ACCESS

Protocol

Visualizing crystal structure evolution of electrode materials upon doping and during charge/discharge cycles in lithium-ion batteries

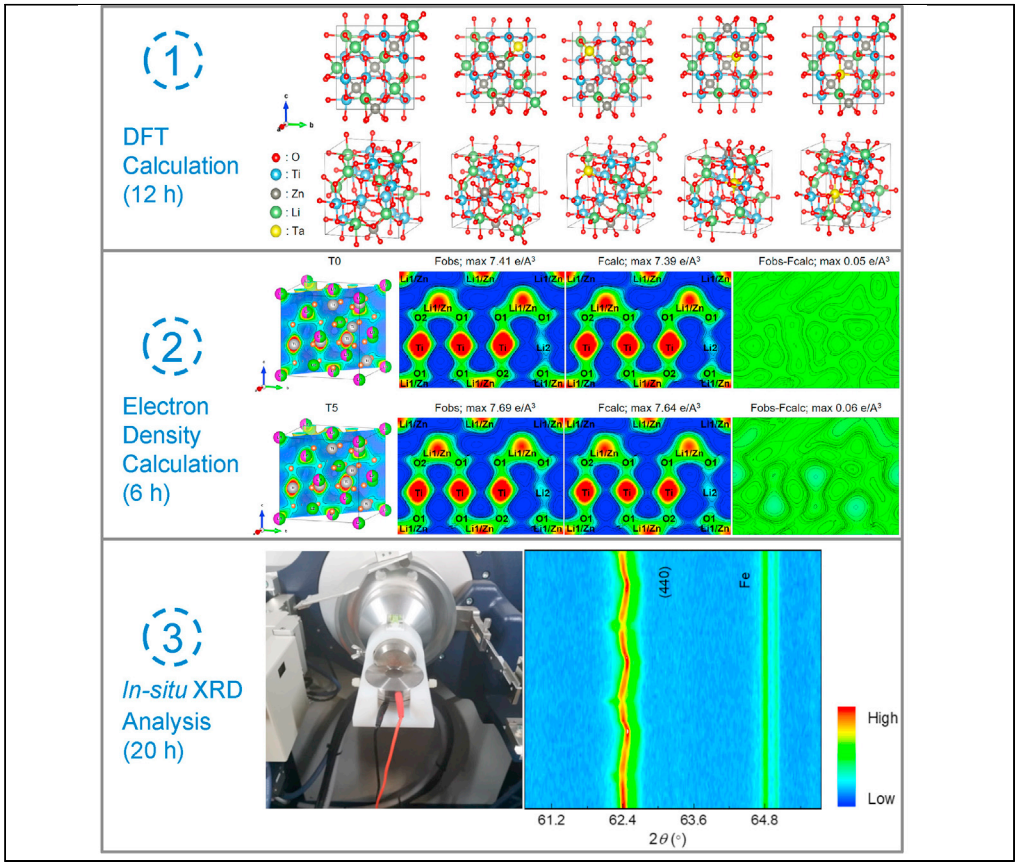

Here we propose a systematic approach to reliably visualize the crystal structure evolution of electrode materials of lithium-ion batteries. Using anodic Ta^{5+}-doped $Li_2ZnTi_3O_8$ (LZTO) spheres as an example, this protocol describes the doping state modeling by density functional theory (DFT) calculation, their crystal structure parameter determination by X-ray diffraction (XRD) refinement, and formation energy by electron density calculation. This protocol also details the *in-situ* XRD analysis approach to visualize the reversibility of Ta^{5+}-doped LZTO during the cycles and the data processing.

Dongwei Ma, Jing Yang, Maykel Manawan, ..., Ting Feng, Yong-Wei Zhang, Jia Hong Pan

pan@ncepu.edu.cn

Highlights

Monodisperse Ta^{5+}-doped $Li_2ZnTi_3O_8$ spheres from TiO_2 spheres as self-template

DFT and electron density calculations for crystal structure parameters

In-situ XRD analysis to visualize crystal structure evolution of electrodes

Ma et al., STAR Protocols *3*, 101099
March 18, 2022
https://doi.org/10.1016/j.xpro.2021.101099

STAR Protocols

CellPress
OPEN ACCESS

Protocol

Visualizing crystal structure evolution of electrode materials upon doping and during charge/discharge cycles in lithium-ion batteries

Dongwei Ma,[1,6] Jing Yang,[2,6] Maykel Manawan,[3,6] Chengfu Yang,[1] Jiahui Li,[1] Yongri Liang,[4] Ting Feng,[5] Yong-Wei Zhang,[2] and Jia Hong Pan[1,7,8,*]

[1]MOE Key Laboratory of Resources and Environmental Systems Optimization, College of Environmental Science and Engineering, North China Electric Power University, Beijing 102206, China

[2]Institute of High Performance Computing, Agency for Science, Technology and Research (A*STAR), 1 Fusionopolis Way, #16-16 Connexis, Singapore 138632, Singapore

[3]Fakultas Teknologi Pertahanan, Universitas Pertahanan Indonesia, Jawa Barat 16810, Indonesia

[4]State Key Lab of Metastable Materials Science and Technology, and School of Materials Science and Engineering, Yanshan University, Qinhuangdao 066012, Hebei, China

[5]School of Metallurgical and Ecological Engineering, University of Science & Technology Beijing, Beijing 100083, China

[6]These authors contributed equally

[7]Technical contact

[8]Lead contact

*Correspondence: pan@ncepu.edu.cn
https://doi.org/10.1016/j.xpro.2021.101099

SUMMARY

Here we propose a systematic approach to reliably visualize the crystal structure evolution of electrode materials of lithium-ion batteries (LIBs) during cyclic charge/discharge process. Using anodic Ta^{5+}-doped $Li_2ZnTi_3O_8$ (LZTO) spheres as an example, this protocol describes the doping state modeling by density functional theory (DFT) calculation, their crystal structure parameter determination by X-ray diffraction (XRD) refinement, and formation energy by electron density calculation. This protocol also details the *in-situ* XRD technique and date processing to visualize the cycling reversibility of Ta^{5+}-doped LZTO.

For complete details on the use and execution of this profile, please refer to Ma et al. (2021).

BEFORE YOU BEGIN

The charge/discharge process of lithium-ion batteries (LIBs) is accompanied by the insertion/extraction of Li^+ into/from the electrode materials. The underlying crystal structure evolution is crucial to the stability and lifetime of LIBs. Here, we present a protocol to visualize the doping state and structure evolution by a combined density functional theory (DFT) calculation, electron density calculation, and *in-situ* XRD technology. We choose Ta^{5+}-doped LZTO spheres as an example to detail our method. Therefore, this protocol starts from its synthesis.

Preparation of hydrous TiO_2 colloidal spheres (HTCS) via sol-gel process

Timing: 4 h

1. Prepare a mixed solution containing ethanol (19.2 g), acetonitrile (12.8 g), DI water (0.15 g), and $NH_3 \cdot H_2O$ (0.068 mL, ~28%). Then, add 4.0 mL of distilled titanium (IV) tetraisopropoxide (TTIP)

into the mixed solution under vigorous stirring. White precipitate of HTCS forms immediately (less than 1 s).

Reagent	Final concentration	Amount
Ethanol	99.99%	24.3 mL
Acetonitrile	99.99%	16.3 mL
DI water	n/a	0.15 mL
$NH_3 \cdot H_2O$	28%	0.068 mL
TTIP	99.99%	4.0 mL
Total	n/a	44.818 mL
Storage: Store for up to 6 months at 25°C.		

Note: Experimental technique is critical to the uniformity of spheres. The stirring should keep vigorous and stable before and after introducing TTIP. We generally use pipette with a 5-mL tip to transfer TTIP. When adding TTIP to the solution, press the plunger to the bottom as quickly as possible when the tip is close to the liquid level.

2. Keep vigorously stirring for 5 min before the aging process. Two different aging processes are available to fully hydrolyze Ti precursors. One is statical aging. That is, stop the stirring and seal the suspension with parafilm and keep it statically for 3 h at room temperature (20°C–25°C). Alternatively, slow down the stirring speed to 100–150 rpm and keep the gentle stirring for 3 h.
3. Centrifuge the suspension solution to collect the white powders, i.e., amorphous HTCS. Wash HTCS with ethanol twice and then water twice, and dry in electric oven.

Preparation of mesoporous anatase TiO_2 spheres (MATS) via microwave-assisted self-template route

Timing: 1 h

4. Redisperse the dried HTCS (0.5 g) in DI water (20 mL). Use microwave irradiation to radiate the formed suspension (Power: 150 W; Temperature: 130°C) for 0.5 h by using CEM Discover SP equipment under continuous stirring. HTCS can be *in-situ* crystallized to MATS. Recover the white powders of MATS by centrifugation and dry in electric oven.

Preparation of Ta^{5+}-doped LZTO spheres using MATS as self-template

Timing: 8 h

5. Ball-milling MATS (0.059 mol), Li_2CO_3 (0.02 mol), zinc acetate (0.02 mol), and Ta_2O_5 (0.0005 mol) with a stoichiometric amount at 150 rpm for 4 h in the 100 mL vessel of the ball-milling jar with ethanol as the dispersant.
6. Calcine the mixed powders at 800°C for 4 h in air, and finally to obtain Ta^{5+}-doped LZTO spheres.

KEY RESOURCES TABLE

REAGENT or RESOURCE	SOURCE	IDENTIFIER
Chemicals, peptides, and recombinant proteins		
Titanium (IV) tetraisopropoxide (>99%)	Sigma-Aldrich	CAS#546-68-9
Ethanol (≥99.7%, HPLC)	Sigma-Aldrich	CAS#64-17-5
Ammonium hydroxide solution (25–28%, GR)	Sigma-Aldrich	CAS#1336-21-6

(*Continued on next page*)

Continued

REAGENT or RESOURCE	SOURCE	IDENTIFIER
Anhydrous Acetonitrile (99.99%, HPLC)	Sigma-Aldrich	CAS#75-05-8
Lithium carbonate (99.99%, metals basis)	Sigma-Aldrich	CAS#554-13-2
Tantalum oxide (99.99%, metals basis)	Sigma-Aldrich	CAS#1314-61-0
Zinc acetate (99.99%, metals basis)	Sigma-Aldrich	CAS#557-34-6
Aeroxide P25	Sigma-Aldrich	CAS#13463-67-7
Hombikat 8602 (~100nm)	Sigma-Aldrich	CAS#1317-80-2
Rutile TiO_2 (~50 nm)	Sigma-Aldrich	CAS#13463-67-7
Critical commercial assays		
Neware 5V10mA battery tester	Neware, China	https://www.neware.com.cn/
In-situ XRD device (LIB-XRD-03C battery case)	Zhongke Wanyuan Technology	http://www.zkwy888.com/
Deposited data		
PDF-4+ 2021	ICDD	https://www.icdd.com/
Software and algorithms		
ZIVE MP1 electrochemical workstation	WonATech Corp., Korea	http://www.wonatech.com/
CHI760E electrochemical workstation	CH Instruments	http://www.chinstr.com/
Neware battery testing system	Neware, China	https://www.neware.com.cn/
VESTA v3.5.7	K. Momma & F. Izumi	http://jp-minerals.org/vesta/en/
DIFFRAC.TOPAS V6	Bruker	https://www.bruker.com/
DIFFRAC.EVA V6	Bruker	https://www.bruker.com/
PROFEX V4.3	Nicola Döbelin	https://www.profex-xrd.org/
RIETAN-FP	Fujio Izumi	http://fujioizumi.verse.jp/
Origin 2020	Originlab	https://www.originlab.com/
Vienna ab-initio simulation package	Hafner group, University of Vienna	https://www.vaspweb.org/
Other		
Discover SP equipment	CEM, USA	Discover SP-D 80
Ball-milling jar	Nanjing Laibu Technology Industrial Co., China	N/A
Be sheet	Zhongke Wanyuan Technology	N/A
Powder X-ray diffraction	Rigaku, Japan	Smartlab SE
Grazing incidence X-ray diffraction	Beijing Synchrotron Radiation Facility	1W2A
Scanning Electron Microscopy	JEOL, Japan	JSM-7800F
Transmission Electron Microscopy	JEOL, Japan	JEM-2010
Oxford X-MAX50 energy dispersive spectrometer	Oxford Instruments, UK	Oxford-X-MAX-50
XPS spectra	Thermo Fisher Scientific Inc., USA	Thermo Kalpha
Raman spectra	Horiba, Japan	T64000
Brunauer-Emmett-Teller	Micromeritics, USA	ASAP 2020 HD88
Thermogravimetry	NETZSCH, Germany	STA 2500

STEP-BY-STEP METHOD DETAILS

The calculation process of DFT

Timing: 12 h

The DFT calculations follow a step-by-step instruction to perform the structure optimization, lattice constant calculation, formation energy calculation and volume calculation.

1. Calculations set up: Perform all the DFT calculations using the plane-wave technique implemented in Vienna ab initio simulation package (Kresse and Hafner, 1993a; 1993b).
   a. Employ the generalized gradient approximation with the Perdew-Burke-Ernzerhof (PBE) functional to describe the exchange-correction potential in all calculations (Blöchl, 1994; Perdew et al., 1996).
   b. Expand wave functions in a plane-wave basis set with a cutoff kinetic energy of 500 eV. Sample their Brillouin zone with 3 × 3 × 3 grid based on the Monkhorst and Pack scheme (Monkhorst and Pack, 1976).

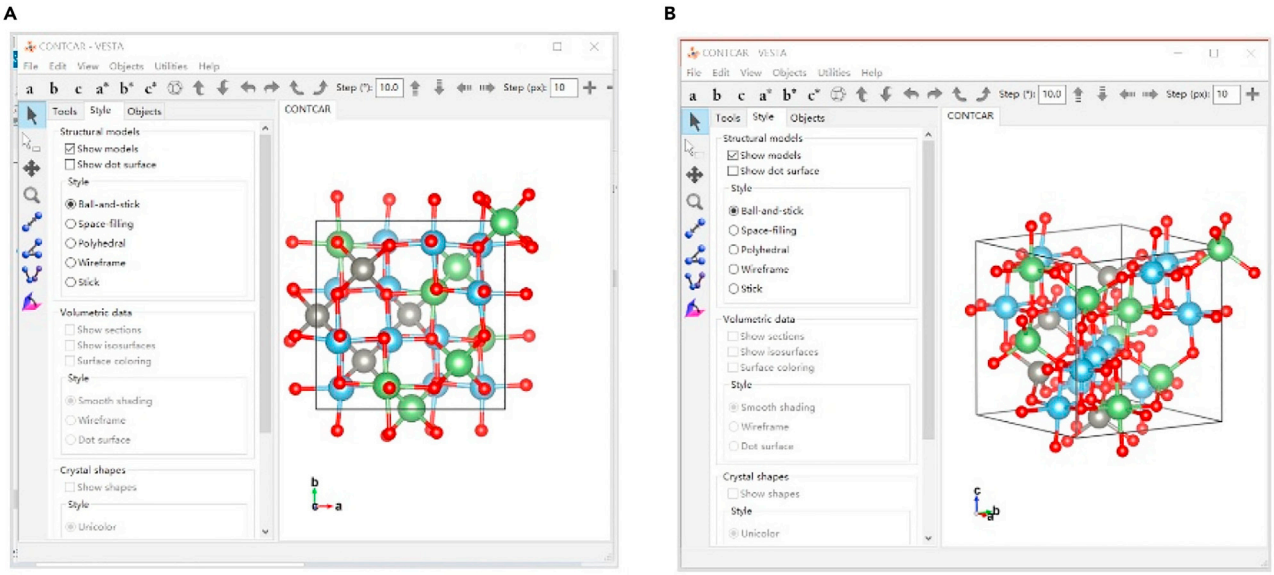

Figure 1. Structure of standard LZTO visualized with the software of VESTA

Red, bule, grey and green spheres represent O, Ti, Zn and Li atoms, respectively.
(A) Top view and (B) Side view.

c. For LZTO model, construct four formula units containing 56 atoms, as visualized with the software of VESTA. Figure 1 shows the view structure of standard LZTO.

2. Structure optimization: Calculations begin with the optimization of standard LZTO.
   a. Perform a full optimization of LZTO that atomic positions, cell shape and cell volume by setting ISIF tag equals to 3 in the INCAR file.
   b. Extract the lattice constant value from the CONTCAR file, which is one of the output files of the calculation. The lattice constant for standard LZTO is 8.38 Å.
   c. The calculated lattice parameters fall in the range of 8.38–8.42 Å, which is in good agreement with our XRD results (8.37 Å for the standard LZTO and 8.38 Å for Ta^{5+}-doped LZTO) and other results reported in the literature (Yang et al., 2017).
3. Possible substitution: There are two possible substitution sites for the guest Ta atom: tetrahedral sites (Li or Zn atoms) or octahedral sites (Li or Ti atoms). So altogether, there are four substitution possibilities: Li (tetrahedral sites) Ta, Zn (tetrahedral sites) Ta, Li (octahedral sites) Ta, and Ti (octahedral sites) Ta. We prepare all these structures and did the structure optimization again with ISIF = 3.

4. Formation energy calculation: After geometry optimization, estimate the formation energy of each possible structures per unit cell (ΔE_f) (the unit cell contains four units of LZTO with periodic boundary conditions) by the following Equations:

$$\Delta E_f = E_{LZTO} - 8 \times E_{Li} - 4 \times E_{Zn} - 12 \times E_{Ti} - 32 \times E_O \quad \text{(Equation 1)}$$

$$\Delta E_{f,\,Li\leftrightarrow Ta} = E_{LZTO,\,Li\leftrightarrow Ta} - 7 \times E_{Li} - 4 \times E_{Zn} - 12 \times E_{Ti} - 32 \times E_O - E_{Ta} \quad \text{(Equation 2)}$$

$$\Delta E_{f,\,Zn\leftrightarrow Ta} = E_{LZTO,\,Zn\leftrightarrow Ta} - 8 \times E_{Li} - 3 \times E_{Zn} - 12 \times E_{Ti} - 32 \times E_O - E_{Ta} \quad \text{(Equation 3)}$$

$$\Delta E_{f,\,Ti\leftrightarrow Mo} = E_{LZTO,\,Ti\leftrightarrow Ta} - 8 \times E_{Li} - 4 \times E_{Zn} - 11 \times E_{Ti} - 32 \times E_O - E_{Ta} \quad \text{(Equation 4)}$$

where E_{LZTO} is the total electronic energy of LZTO unit cell obtained from the OSZICAR file which is another output file of the calculation. E_{Li}, E_{Zn}, E_{Ti}, and E_{Ta} are the total electronic energies of Li, Zn, Ti, and Ta atoms, respectively.

	Standard	Tetrahedral site substitution		Octahedral site substitution	
		Zn ↔Ta	Li ↔Ta	Li ↔Ta	Ti ↔Ta
Optimized Structure	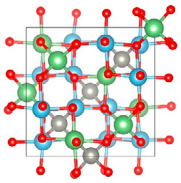	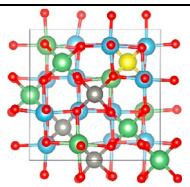	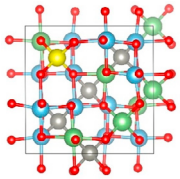	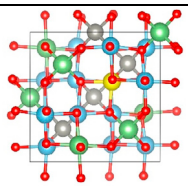	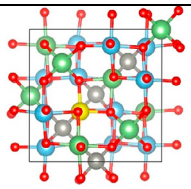
		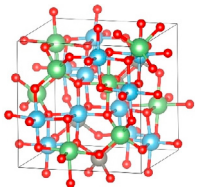	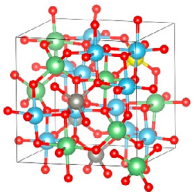	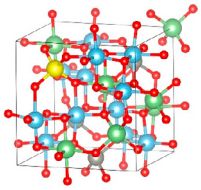	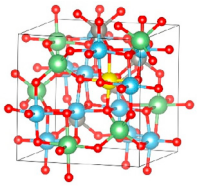
		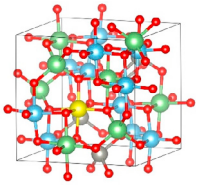			
Unit Cell	$Li_8Zn_4Ti_{12}O_{32}$	$Li_8Zn_3Ti_{12}TaO_{32}$	$Li_7Zn_4Ti_{12}TaO_{32}$	$Li_7Zn_4Ti_{12}TaO_{32}$	$Li_8Zn_4Ti_{11}TaO_{32}$
Lattice (Å)	8.38	8.41	8.42	8.41	8.41
Volume ($Å^3$)	588.05	594.66	595.49	597.23	591.80
E_f (eV)	-35.18	-35.43	-34.82	-34.82	-35.72

Figure 2. The optimized structure of all possible Ta-substituted LZTO and their lattice constant
Red, bule, grey, green and yellow spheres represent O, Ti, Zn, Li and Ta atoms, respectively (Ma et al., 2021)

a. Estimate above data from the energy of pure metal bulk. E_O is the total electronic energies of O atom which is half of the total energy of O_2.
b. Note that the total electronic energies of Li, Zn, Ti, and Ta atoms calculated by single atom are not applicable.
c. Because such an isolate atom is far from the experiments that in the real material, the atoms interact with the surrounding. Li ↔ Ta, Zn ↔ Ta, and Ti ↔ Ta refers to the substitutions of Ta for Li, Zn, and Ti, respectively. Figure 2 summarizes the optimized structures, lattice constant, volume, and E_f.

The calculation process of the electron density map

Timing: 6 h

Determine the electron density distribution using TOPAS (Rietveld refinement), PROFEX (Fourier synthesis), and RIETAN-FP (Maximum Entropy Method). Firstly, the structural data can be refined using TOPAS. The refined result can be output as a crystallographic information file (*.CIF), which is then used as an input Profex-BGMN and RIETAN-FP.

The Rietveld refinement procedure in TOPAS is as follows:

5. Identify the structural files (*.CIF) from ICDD PDF-4+ 2021 database using DIFFRAC.EVA V6 (Bruker AXS, 2021; Gates-Rector and Blanton, 2019).
6. Set the wavelength of 1.5405Å and take the instrument configuration information from the instrument configuration.
7. Perform Rietveld refinements by carefully refine the lattice parameters, atomic position, occupancy, and thermal parameters. The step-by-step refinement process and checking follow (McCusker et al., 1999) and (Toby, 2006), respectively.

The Fourier synthesis procedure in PROFEX is as follows:

8. Use the TOPAS structural output file (*.CIF) as a structural input file (*.STR) in PROFEX.
9. The instrument configuration file (*.SAV) use the wavelength of 1.5405 Å and information from instrument configuration.
10. Perform the refinement by fixing all structural parameters. Inspect the graphics and the *R*-factors, then compared them to TOPAS. If not satisfied, repeat step 9 by modifying the instrument configuration, preferred orientation, crystallite size, and strain.
11. Create the electron density distribution by right click the *.STR in 'SAV tab' and select 'add RES-OUT and FCOUT file', run the refinement and go to 'Tools' and select the 'Electron Density Map'.

The Maximum Entropy Method procedure in RIETAN-FP is as follow:

12. Using VESTA, open the CIF output from TOPAS. In 'Utilities tab', select 'Powder Diffraction Pattern' to create the RIETAN-FP input file (*.INS).
13. Open the *.INS file by 'MARUO editor', check the instrument following item to follow the instrument configuration and Rietveld refinement: Radiation (NBEAM=1), Analytical Method (NMODE=0), Wavelength (NTARG=4), Geometry (NTRAN=0), Profile Function (NPRFN=0), Asymmetric (NASYM=1), Peak-shift function (NSHIFT=4), Voxel numbers (NVOXA=132, NVOXB=132, NVOXC=100), Diffraction data (NINT=1), Background (NRANGE=0), Update of hoge.ins (NUPDT=1), Mem analysis (NMEM=1).
14. Run RIETAN, inspect the graphics and the R-factor, then compare it to TOPAS. If not satisfied, check the profile function, refine preferred orientation, add more background terms, etc.
15. Run Dysnomia and inspect the electron density by opening the *.PGRID file in VESTA. Visually inspect the density by insert and comparing with the structure output file (*.CIF) from TOPAS. If not satisfied, repeat step 13 by modifying the structural model.

Note: Explain the step-by-step manual in detail within TOPAS 6 tutorial (Bruker AXS, 2017), PROFEX user manual version 4.3 (Doebelin and Kleeberg, 2015), and Multi-Purpose Pattern-Fitting System RIETAN-FP (Izumi and Momma, 2007). Herein we provide a Methods video S1 in the Supplemental information to show how we perform the refinement and visualization.

The preparation of Ta^{5+}-doped LZTO slurry for LIB anode construction

Timing: 20 h

Coat slurries on the Cu foils and Be pieces and serve as the anodes for *in-situ* XRD analyses, respectively.

16. Mixing at a weight ratio of 8:1:1 of active Ta^{5+}-doped LZTO nanomaterial, super P, and polyvinylidene fluoride (PVDF) with the addition of N-Methyl-2-pyrollidone (NMP) and ball-milling for 1 h.
17. Utilize Be sheet with a diameter of 20 mm as the window for the penetrating of X-ray. A Cu foil with a 14-mm-diameter hole covers the Be sheet. The slurry uniformly coating on Cu foil by doctor blade method. After removing the Cu foil, the slurry with a diameter of 14 mm is deposited on the Be sheet.
18. Dry the Be sheet with slurry in vacuum at 120°C for 12 h. Press the dried black electrodes slightly for measurement.

⚠ CRITICAL: When preparing and coating the slurry, and handling the Be sheet, perform all the operations in a chemical hood with the protection of gloves.

19. Assemble the *in-situ* XRD device in a glove box, and the assembly sequence is Be sheet with the electrode, two drops of electrolyte, Celgard 2300 separator, two drops of electrolyte, lithium piece, and counter electrode, as shown in Figure 3.
20. Process the collected XRD patterns and make the 2D contour plots using Origin software, as shown in Figure 4.

Note: Be sheet can be reused as the X-ray window for dozens of times.

Optional: Use different kinds of X-ray window, such as quartz window and Kapton membrane.

EXPECTED OUTCOMES

Ti site is most easily replaced by Ta^{5+} compared with Li and Zn site. After Ta^{5+} doping, the stability of crystal structure is increased during the cyclic charge/discharge process. The calculated formation energies are summarized in Figure 2. The formation energy for standard LZTO is calculated to be −35.18 eV per formula. And the formation energies for the four possible Ta^{5+}-doped LZTO are −35.43 eV, −34.82 eV, −34.82 eV and −35.72 eV for Zn ↔Ta, tetrahedral Li ↔Ta, octahedral Li ↔Ta and Ti↔Ta substation. The Ti↔Ta substitution is more favorable than others because it gives the lowest formation energy. It is in line with our XRD results that the Ta^{5+} ions can be uniformly doped into crystal lattices of LZTO through the Ti↔Ta substitution.

The volume of the calculated material can be found in the OUTCAR file. As presented in Figure 2, the calculated volume of the standard LZTO is 588.05 $Å^3$, which is slightly increased to 591.80 $Å^3$ after the Ta^{5+} substitution. Such expansion in volume is beneficial for the formation of rapid electronic transportation channels. As shown in Figure 4, the (440) diffraction peak of Ta^{5+}-doped LZTO shifts reversibly during the cyclic charge/discharge process, which means their high reversibility for Li^+ ion de/intercalation. The superiority in the structural stability of Ta^{5+}-doped LZTO is mainly ascribed to their larger unit cell volume with higher tolerances in structural expansion and contraction during the cyclic lithiation and delithiation processes.

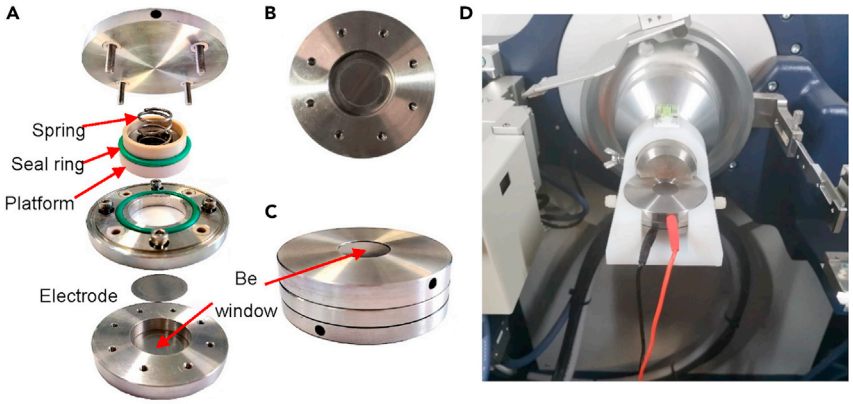

Figure 3. Preparing the *in-situ* XRD device
(A) Internal assembly of *in-situ* XRD device.
(B) Be sheet with the electrode (14 mm) in the module.
(C) The assembled cell ready for the *in-situ* XRD test.
(D) The assembled device placed on the XRD sample holder for the *in-situ* analysis.

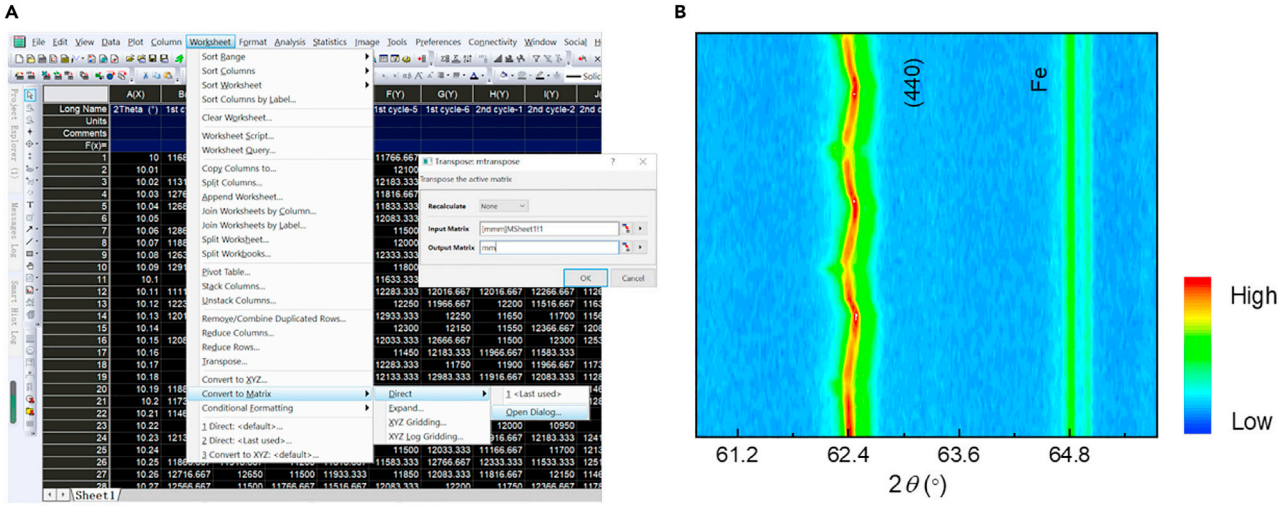

Figure 4. Processing *in-situ* XRD data to create 2D contour plots

(A) Screenshot of Origin program operation to generate 2D contour plots.

(B) The resultant 2D contour plots of Ta^{5+}-doped LZTO anodes.

LIMITATIONS

The main limitation to execute this protocol is the instruments and facilities of *in-situ* XRD measurement. The quality Be sheet window depends on the purity, thickness and service life. We suggest using the unused Be window with a thickness of 15 mm for the *in-situ* XRD test.

TROUBLESHOOTING

Problem 1

When the slurry is coated on the Be sheet, the electrode may peel off from Be sheet after drying, due to the untight contact between the slurry and the Be sheet. (In step 18 of the preparation of Ta^{5+}-doped LZTO slurry for LIB anode construction)

Potential solution

Try to decrease the drying temperature (e.g., ~50°C), or change the weight proportion of active materials, conductive carbon (Carbon ECP-600JD), and PVDF binder (HSV900, average molecular weight: ~1,000,000 g/mol) to 7:1:2 since the increase in PVDF dosage is helpful to the adhesion.

Problem 2

During the *in-situ* XRD testing, the intensity of XRD peaks for the electrode materials might be too low since the electrode is too thin. (In step 19 of the preparation of Ta^{5+}-doped LZTO slurry for LIB anode construction)

Potential solution

When coating the viscous slurry consisting of active materials, conductive carbon, PVDF binder, and NMP on Cu foil by doctor blading, the thickness of the electrode can be controlled by adjusting the size of the scraper. Try to increase the thickness of the slurry when coated on the Be sheet. The optimal thickness should be in range of 30–50 μm.

Problem 3

During the *in-situ* XRD test, abnormal charging and discharging might happen due to the fracture of the electrode. (In step 19 of the preparation of Ta^{5+}-doped LZTO slurry for LIB anode construction)

Potential solution

During the *in-situ* XRD device assembly, be careful not to over tighten the set screws as the device can not work properly under the overhigh pressure. Control the screw tightness to about 80%.

Problem 4

During the *in-situ* XRD test, electrolyte leakage may occur. (In step 19 of the preparation of Ta^{5+}-doped LZTO slurry for LIB anode construction)

Potential solution

The dosage of electrolyte should be strictly controlled, which, for example, is generally less than 50 μL in our module.

Problem 5

During the *in-situ* XRD test, the electrochemical performance will be low, compared to that in the coin cell. This is because the electrolyte does not infiltrate the electrode sufficiently. (In step 19 of the preparation of Ta^{5+}-doped LZTO slurry for LIB anode construction)

Potential solution

After assembled, the *in-situ* XRD device should be left statically for more than 6 h before the cyclic charge/discharge process.

RESOURCE AVAILABILITY

Lead contact

Further information and requests for resources and reagents should be directed to and will be fulfilled by the lead contact, Jia Hong Pan (pan@ncepu.edu.cn)

Materials availability

This study did not generate new unique reagents.

Data and code availability

We did not generate any dataset or code.

SUPPLEMENTAL INFORMATION

Supplemental information can be found online at https://doi.org/10.1016/j.xpro.2021.101099.

ACKNOWLEDGMENTS

This work is supported by National Natural Science Foundation of China (No. 51772094) and National 111 Project (No. B16016). The authors gratefully acknowledge the cooperation of the beamline scientists at BSRF-1W1A beamline.

AUTHOR CONTRIBUTIONS

D.M., J.Y., and M.M. drafted the manuscript. D.M., J.Y., M.M., C.Y., J.L, Y.L., T.F., and Y.W.Z. conducted the tests. J.H.P reviewed and edited the writing.

DECLARATION OF INTERESTS

The authors declare no competing interests.

REFERENCES

Blöchl, P.E. (1994). Projector augmented-wave method. Phys. Rev. B *50*, 17953–17979. https://doi.org/10.1103/PhysRevB.50.17953.

Bruker AXS. (2017). General Profile Analysis Techniques. TOPAS 6 Tutorial (Karlsruhe, Germany: Bruker AXS GmbH), pp. 115–123.

Bruker AXS. (2021). Performing a Search/Match Operation. Diffrac. EVA Tutorial (Karlsruhe, Germany: Bruker AXS GmbH), pp. 3–9.

Doebelin, N., and Kleeberg, R. (2015). *Profex*: a graphical user interface for the Rietveld refinement program *BGMN*. J. Appl. Crystallogr. *48*, 1573–1580. https://doi.org/10.1107/S1600576715014685.

Gates-Rector, S., and Blanton, T. (2019). The Powder Diffraction File: a quality materials characterization database. Powder Diffr. *34*, 352–360. https://doi.org/10.1017/S0885715619000812.

Izumi, F., and Momma, K. (2007). Three-dimensional visualization in powder diffraction. Solid State Phenom. *130*, 15–20. https://doi.org/10.4028/www.scientific.net/SSP.130.15.

Kresse, G., and Hafner, J. (1993a). Ab initio molecular dynamics for open-shell transition metals. Phys. Rev. B *48*, 13115–13118. https://doi.org/10.1103/PhysRevB.48.13115.

Kresse, G., and Hafner, J. (1993b). Ab initio molecular dynamics for liquid metals. Phys. Rev. B *47*, 558–561. https://doi.org/10.1103/PhysRevB.47.558.

Ma, D., Li, J., Yang, J., Yang, C., Manawan, M., Liang, Y., Feng, T., Zhang, Y.-W., and Pan, J.H. (2021). Solid-state self-template synthesis of Ta-doped $Li_2ZnTi_3O_8$ spheres for efficient and durable lithium storage. iScience *24*, 102991. https://doi.org/10.1016/j.isci.2021.102991.

McCusker, L.B., Von Dreele, R.B., Cox, D.E., Louër, D., and Scardi, P. (1999). Rietveld refinement guidelines. J. Appl. Crystallogr. *32*, 36–50. https://doi.org/10.1107/S0021889898009856.

Monkhorst, H.J., and Pack, J.D. (1976). Boosting electrochemical water splitting: via ternary NiMoCo hybrid nanowire arrays. Phys. Rev. B *13*, 5188–5192. https://doi.org/10.1039/c8ta11250a.

Perdew, J.P., Burke, K., and Ernzerhof, M. (1996). Generalized gradient approximation made simple. Phys. Rev. Lett. *77*, 3865–3868. https://doi.org/10.1103/PhysRevLett.77.3865.

Toby, B.H. (2006). *R* factors in Rietveld analysis: How good is good enough? Powder Diffr. *21*, 67–70. https://doi.org/10.1154/1.2179804.

Yang, H., Park, J., Kim, C.S., Xu, Y.H., Zhu, H.L., Qi, Y.X., Yin, L., Li, H., Lun, N., and Bai, Y.J. (2017). Uniform surface modification of $Li_2ZnTi_3O_8$ by liquated Na_2MoO_4 to boost electrochemical performance. ACS Appl. Mater. Interfaces *9*, 43603–43613. https://doi.org/10.1021/acsami.7b12208.